Improved measurement of the B^0_d–$\overline{B}^0\_d$ Oscillation frequency

D. Buskulic, I. de Bonis, D. Decamp, P. Ghez, C. Goy, J P. Lees, A. Lucotte, M N. Minard, J Y. Nief, P. Odier, et al.

EUROPEAN ORGANIZATION FOR NUCLEAR RESEARCH

CERN–PPE/96–102
17 July 1996

Improved measurement of the B^0_d–$\overline{B}^0_d$ oscillation frequency

The ALEPH Collaboration[1]

Abstract

The time dependence of B^0_d–$\overline{B}^0_d$ oscillations is measured by the ALEPH experiment at LEP, using three techniques, two of which are updates of previous measurements. In all cases the charge of the decaying b quark and its decay time are measured in one hemisphere of the event; the quark charge at production is tagged mainly using the opposite hemisphere. The first method uses the charge correlation between a D^{*-} and a lepton in the opposite hemisphere; if no lepton is present, the produced quark charge is determined from the hemisphere charges. In the second method, the decay time is measured using a lepton in one hemisphere and the initial state is inferred from the opposite-hemisphere jet charge. The third method uses a lepton in each hemisphere. The data used were collected from 1991 to 1994. The combined result is $\Delta m_d = 0.436 \pm 0.033\,\mathrm{ps}^{-1}$.

(Submitted to Z. Phys. C)

[1]See the following pages for the list of authors.

The ALEPH Collaboration

D. Buskulic, I. De Bonis, D. Decamp, P. Ghez, C. Goy, J.-P. Lees, A. Lucotte, M.-N. Minard, J.-Y. Nief, P. Odier, B. Pietrzyk

Laboratoire de Physique des Particules (LAPP), IN^{2}P^3-CNRS, 74019 Annecy-le-Vieux Cedex, France

M.P. Casado, M. Chmeissani, J.M. Crespo, M. Delfino, I. Efthymiopoulos,[1] E. Fernandez, M. Fernandez-Bosman, Ll. Garrido,[15] A. Juste, M. Martinez, S. Orteu, C. Padilla, I.C. Park, A. Pascual, J.A. Perlas, I. Riu, F. Sanchez, F. Teubert

Institut de Fisica d'Altes Energies, Universitat Autonoma de Barcelona, 08193 Bellaterra (Barcelona), Spain[7]

A. Colaleo, D. Creanza, M. de Palma, G. Gelao, M. Girone, G. Iaselli, G. Maggi, M. Maggi, N. Marinelli, S. Nuzzo, A. Ranieri, G. Raso, F. Ruggieri, G. Selvaggi, L. Silvestris, P. Tempesta, A. Tricomi,[3] G. Zito

Dipartimento di Fisica, INFN Sezione di Bari, 70126 Bari, Italy

X. Huang, J. Lin, Q. Ouyang, T. Wang, Y. Xie, R. Xu, S. Xue, J. Zhang, L. Zhang, W. Zhao

Institute of High-Energy Physics, Academia Sinica, Beijing, The People's Republic of China[8]

R. Alemany, A.O. Bazarko, G. Bonvicini,[23] P. Bright-Thomas, M. Cattaneo, P. Comas, P. Coyle, H. Drevermann, R.W. Forty, M. Frank, R. Hagelberg, J. Harvey, P. Janot, B. Jost, E. Kneringer, J. Knobloch, I. Lehraus, G. Lutters, E.B. Martin, P. Mato, A. Minten, R. Miquel, Ll.M. Mir,[2] L. Moneta, T. Oest,[20] A. Pacheco, J.-F. Pusztaszeri, F. Ranjard, P. Rensing,[12] G. Rizzo, L. Rolandi, D. Schlatter, M. Schmelling,[24] M. Schmitt, O. Schneider, W. Tejessy, I.R. Tomalin, A. Venturi, H. Wachsmuth, A. Wagner

European Laboratory for Particle Physics (CERN), 1211 Geneva 23, Switzerland

Z. Ajaltouni, A. Barrès, C. Boyer, A. Falvard, P. Gay, C . Guicheney, P. Henrard, J. Jousset, B. Michel, S. Monteil, J-C. Montret, D. Pallin, P. Perret, F. Podlyski, J. Proriol, P. Rosnet, J.-M. Rossignol

Laboratoire de Physique Corpusculaire, Université Blaise Pascal, IN^{2}P^3-CNRS, Clermont-Ferrand, 63177 Aubière, France

T. Fearnley, J.B. Hansen, J.D. Hansen, J.R. Hansen, P.H. Hansen, B.S. Nilsson, B. Rensch, A. Wäänänen

Niels Bohr Institute, 2100 Copenhagen, Denmark[9]

A. Kyriakis, C. Markou, E. Simopoulou, I. Siotis, A. Vayaki, K. Zachariadou

Nuclear Research Center Demokritos (NRCD), Athens, Greece

A. Blondel, G. Bonneaud, J.C. Brient, P. Bourdon, A. Rougé, M. Rumpf, A. Valassi,[6] M. Verderi, H. Videau[21]

Laboratoire de Physique Nucléaire et des Hautes Energies, Ecole Polytechnique, IN^{2}P^3-CNRS, 91128 Palaiseau Cedex, France

D.J. Candlin, M.I. Parsons

Department of Physics, University of Edinburgh, Edinburgh EH9 3JZ, United Kingdom[10]

E. Focardi,[21] G. Parrini

Dipartimento di Fisica, Università di Firenze, INFN Sezione di Firenze, 50125 Firenze, Italy

M. Corden, C. Georgiopoulos, D.E. Jaffe

Supercomputer Computations Research Institute, Florida State University, Tallahassee, FL 32306-4052, USA [13,14]

A. Antonelli, G. Bencivenni, G. Bologna,[4] F. Bossi, P. Campana, G. Capon, D. Casper, V. Chiarella, G. Felici, P. Laurelli, G. Mannocchi,[5] F. Murtas, G.P. Murtas, L. Passalacqua, M. Pepe-Altarelli

Laboratori Nazionali dell'INFN (LNF-INFN), 00044 Frascati, Italy

L. Curtis, S.J. Dorris, A.W. Halley, I.G. Knowles, J.G. Lynch, V. O'Shea, C. Raine, P. Reeves, J.M. Scarr, K. Smith, P. Teixeira-Dias, A.S. Thompson, F. Thomson, S. Thorn, R.M. Turnbull

Department of Physics and Astronomy, University of Glasgow, Glasgow G12 8QQ,United Kingdom[10]

U. Becker, C. Geweniger, G. Graefe, P. Hanke, G. Hansper, V. Hepp, E.E. Kluge, A. Putzer, M. Schmidt, J. Sommer, H. Stenzel, K. Tittel, S. Werner, M. Wunsch

Institut für Hochenergiephysik, Universität Heidelberg, 69120 Heidelberg, Fed. Rep. of Germany[16]

D. Abbaneo, R. Beuselinck, D.M. Binnie, W. Cameron, P.J. Dornan, A. Moutoussi, J. Nash, J.K. Sedgbeer, A.M. Stacey, M.D. Williams

Department of Physics, Imperial College, London SW7 2BZ, United Kingdom[10]

G. Dissertori, P. Girtler, D. Kuhn, G. Rudolph

Institut für Experimentalphysik, Universität Innsbruck, 6020 Innsbruck, Austria[18]

A.P. Betteridge, C.K. Bowdery, P. Colrain, G. Crawford, A.J. Finch, F. Foster, G. Hughes, T. Sloan, M.I. Williams

Department of Physics, University of Lancaster, Lancaster LA1 4YB, United Kingdom[10]

A. Galla, I. Giehl, A.M. Greene, C. Hoffmann, K. Jakobs, K. Kleinknecht, G. Quast, B. Renk, E. Rohne, H.-G. Sander, P. van Gemmeren, C. Zeitnitz

Institut für Physik, Universität Mainz, 55099 Mainz, Fed. Rep. of Germany[16]

J.J. Aubert,[21] A.M. Bencheikh, C. Benchouk, A. Bonissent, G. Bujosa, D. Calvet, J. Carr, C. Diaconu, F. Etienne, N. Konstantinidis, P. Payre, D. Rousseau, M. Talby, A. Sadouki, M. Thulasidas, K. Trabelsi

Centre de Physique des Particules, Faculté des Sciences de Luminy, IN^{2}P^3-CNRS, 13288 Marseille, France

M. Aleppo, F. Ragusa[21]

Dipartimento di Fisica, Università di Milano e INFN Sezione di Milano, 20133 Milano, Italy

C. Bauer, R. Berlich, W. Blum, V. Büscher, H. Dietl, F. Dydak,[21] G. Ganis, C. Gotzhein, H. Kroha, G. Lütjens, G. Lutz, W. Männer, H.-G. Moser, R. Richter, A. Rosado-Schlosser, S. Schael, R. Settles, H. Seywerd, R. St. Denis, H. Stenzel, W. Wiedenmann, G. Wolf

Max-Planck-Institut für Physik, Werner-Heisenberg-Institut, 80805 München, Fed. Rep. of Germany[16]

J. Boucrot, O. Callot, Y. Choi,[26] A. Cordier, M. Davier, L. Duflot, J.-F. Grivaz, Ph. Heusse, A. Höcker, A. Jacholkowska, M. Jacquet, D.W. Kim,[19] F. Le Diberder, J. Lefrançois, A.-M. Lutz, I. Nikolic, H.J. Park,[19] M.-H. Schune, S. Simion, J.-J. Veillet, I. Videau, D. Zerwas

Laboratoire de l'Accélérateur Linéaire, Université de Paris-Sud, IN^{2}P^3-CNRS, 91405 Orsay Cedex, France

P. Azzurri, G. Bagliesi, G. Batignani, S. Bettarini, C. Bozzi, G. Calderini, M. Carpinelli, M.A. Ciocci, V. Ciulli, R. Dell'Orso, R. Fantechi, I. Ferrante, L. Foà,[1] F. Forti, A. Giassi, M.A. Giorgi, A. Gregorio, F. Ligabue, A. Lusiani, P.S. Marrocchesi, A. Messineo, F. Palla, G. Sanguinetti, A. Sciabà, P. Spagnolo, J. Steinberger, R. Tenchini, G. Tonelli,[25] C. Vannini, P.G. Verdini, J. Walsh

Dipartimento di Fisica dell'Università, INFN Sezione di Pisa, e Scuola Normale Superiore, 56010 Pisa, Italy

G.A. Blair, L.M. Bryant, F. Cerutti, J.T. Chambers, Y. Gao, M.G. Green, T. Medcalf, P. Perrodo, J.A. Strong, J.H. von Wimmersperg-Toeller

Department of Physics, Royal Holloway & Bedford New College, University of London, Surrey TW20 OEX, United Kingdom[10]

D.R. Botterill, R.W. Clifft, T.R. Edgecock, S. Haywood, P. Maley, P.R. Norton, J.C. Thompson, A.E. Wright

Particle Physics Dept., Rutherford Appleton Laboratory, Chilton, Didcot, Oxon OX11 OQX, United Kingdom[10]

B. Bloch-Devaux, P. Colas, S. Emery, W. Kozanecki, E. Lançon, M.C. Lemaire, E. Locci, B. Marx, P. Perez, J. Rander, J.-F. Renardy, A. Roussarie, J.-P. Schuller, J. Schwindling, A. Trabelsi, B. Vallage

CEA, DAPNIA/Service de Physique des Particules, CE-Saclay, 91191 Gif-sur-Yvette Cedex, France[17]

S.N. Black, J.H. Dann, R.P. Johnson, H.Y. Kim, A.M. Litke, M.A. McNeil, G. Taylor

Institute for Particle Physics, University of California at Santa Cruz, Santa Cruz, CA 95064, USA[22]

C.N. Booth, R. Boswell, C.A.J. Brew, S. Cartwright, F. Combley, A. Koksal, M. Letho, W.M. Newton, J. Reeve, L.F. Thompson

Department of Physics, University of Sheffield, Sheffield S3 7RH, United Kingdom[10]

A. Böhrer, S. Brandt, G. Cowan, C. Grupen, J. Minguet-Rodriguez, F. Rivera, P. Saraiva, L. Smolik, F. Stephan,

Fachbereich Physik, Universität Siegen, 57068 Siegen, Fed. Rep. of Germany[16]

M. Apollonio, L. Bosisio, R. Della Marina, G. Giannini, B. Gobbo, G. Musolino

Dipartimento di Fisica, Università di Trieste e INFN Sezione di Trieste, 34127 Trieste, Italy

J. Rothberg, S. Wasserbaech

Experimental Elementary Particle Physics, University of Washington, WA 98195 Seattle, U.S.A.

S.R. Armstrong, P. Elmer, Z. Feng,[27] D.P.S. Ferguson, Y.S. Gao,[28] S. González, J. Grahl, T.C. Greening, O.J. Hayes, H. Hu, P.A. McNamara III, J.M. Nachtman, W. Orejudos, Y.B. Pan, Y. Saadi, I.J. Scott, A.M. Walsh,[29] Sau Lan Wu, X. Wu, J.M. Yamartino, M. Zheng, G. Zobernig

Department of Physics, University of Wisconsin, Madison, WI 53706, USA[11]

---

[1] Now at CERN, 1211 Geneva 23, Switzerland.
[2] Supported by Dirección General de Investigación Científica y Técnica, Spain.
[3] Also at Dipartimento di Fisica, INFN, Sezione di Catania, Catania, Italy.
[4] Also Istituto di Fisica Generale, Università di Torino, Torino, Italy.
[5] Also Istituto di Cosmo-Geofisica del C.N.R., Torino, Italy.
[6] Supported by the Commission of the European Communities, contract ERBCHBICT941234.
[7] Supported by CICYT, Spain.
[8] Supported by the National Science Foundation of China.
[9] Supported by the Danish Natural Science Research Council.
[10] Supported by the UK Particle Physics and Astronomy Research Council.
[11] Supported by the US Department of Energy, grant DE-FG0295-ER40896.
[12] Now at Dragon Systems, Newton, MA 02160, U.S.A.
[13] Supported by the US Department of Energy, contract DE-FG05-92ER40742.
[14] Supported by the US Department of Energy, contract DE-FC05-85ER250000.
[15] Permanent address: Universitat de Barcelona, 08208 Barcelona, Spain.
[16] Supported by the Bundesministerium für Forschung und Technologie, Fed. Rep. of Germany.
[17] Supported by the Direction des Sciences de la Matière, C.E.A.
[18] Supported by Fonds zur Förderung der wissenschaftlichen Forschung, Austria.
[19] Permanent address: Kangnung National University, Kangnung, Korea.
[20] Now at DESY, Hamburg, Germany.
[21] Also at CERN, 1211 Geneva 23, Switzerland.
[22] Supported by the US Department of Energy, grant DE-FG03-92ER40689.
[23] Now at Wayne State University, Detroit, MI 48202, USA.
[24] Now at Max-Plank-Institüt für Kernphysik, Heidelberg, Germany.
[25] Also at Istituto di Matematica e Fisica, Università di Sassari, Sassari, Italy.
[26] Permanent address: Sung Kyun Kwon University, Suwon, Korea.
[27] Now at The Johns Hopkins University, Baltimore, MD 21218, U.S.A.
[28] Now at Harvard University, Cambridge, MA 02138, U.S.A.
[29] Now at Rutgers University, Piscataway, NJ 08855-0849, U.S.A.

1 Introduction

Observed B^0 states are linear combinations of two mass eigenstates. The probability for a B^0 meson to decay in the originally produced (unmixed) state, or in the opposite (mixed) state, is

$$P_{\mathrm{u,m}} = \frac{\Gamma}{2} \mathrm{e}^{-\Gamma t}(1 \pm \cos \Delta m t), \tag{1}$$

where the oscillation frequency is given by Δm, the mass difference between mass eigenstates, and where the decay rate Γ is expected to be nearly the same for the two states.

The measurement of the oscillation frequency requires the identification of the initial and final states of the B^0 (particle or antiparticle) as well as the measurement of the B^0 decay time. Direct observation of the time dependence of B^0_d oscillations was first reported by the ALEPH Collaboration [1]. The measurement of Δm_d has since been considerably refined [2, 3, 4].

In this paper three separate measurements of the B^0_d oscillation frequency are presented. After a brief description of the ALEPH detector in the next section, Section 3 updates the analysis first described in Ref. [1], based on the $B^0_d \to D^{*-} X$ channel, and extends it by tagging the initial state of the B^0_d using jet charge when no opposite-hemisphere lepton is available.

Section 4 presents a new analysis using inclusive lepton-jet events, containing at least one high transverse-momentum lepton. Here, the final state of the b hadron is determined from the charge of its decay lepton, and its flight time is measured using an inclusive vertexing technique and an estimate of the original b hadron momentum. The charge of the b quark at production time is inferred from the jet charge in the opposite hemisphere.

Section 5 provides an update of the dilepton analysis originally published in Ref. [2]. The three measurements are combined in Section 6, taking into account the correlations between systematic uncertainties affecting the dilepton and lepton-jet measurements.

2 The ALEPH detector and event selection

The ALEPH detector operates at the LEP electron positron storage ring and combines accurate tracking, calorimetry, and particle identification capabilities. Extensive descriptions of the design and performance of the detector can be found in Refs. [5, 6], and only a brief summary of the salient features is given here.

Immediately surrounding the beryllium beam pipe, a double-sided silicon vertex detector is installed. It provides a single-hit resolution of 12 μm at normal incidence in both the $r\phi$ and z directions, and covers 85% of the solid angle. Radially outwards, the vertex detector is followed by an eight-layer drift chamber (ITC), and by a time projection chamber (TPC) which provides tracking information and particle identification via dE/dx. The TPC is surrounded by a projective electromagnetic calorimeter, followed by a 1.5 T superconducting solenoid. The iron return yoke of the magnet is equipped with layers of streamer tubes, which form a hadron calorimeter and provide muon identification. Combined measurements from the tracking system and the calorimeters provide energy flow information. Outside the yoke, completing the muon identification system, are two further double layers of streamer tubes.

In all the analyses discussed below, events are selected from the approximately three million hadronic Z decays collected by ALEPH in the years 1991 to 1994, that satisfy the criteria of Ref. [7]. The Monte Carlo simulations for the analyses described in this paper

use the ALEPH generator HVFL [8], based on the Lund parton-shower model (JETSET 7.3) [9].

3 D^* method

This section describes the measurement of the mixing parameter Δm_d through the observation of oscillations in the particle/antiparticle state of $B^0_d \to D^{*-}X$ final states[2] as a function of their decay distance. The final charge state and the decay length of the B^0_d are inferred from, respectively, the charge of the D^* and the distance between the event primary vertex and the decay vertex of the D^0 produced in the D^* decay. The initial charge state is taken from that of a lepton from semileptonic b decay in the event hemisphere opposite to that of the D^*. If no such lepton is identified, the initial charge state is determined from the momentum-weighted jet charges in the two event hemispheres. Same-sign D^* and lepton (or jet) charges tag the event as "unmixed"; opposite charges indicate a "mixed" event.

3.1 D^0 selection and reconstruction

B^0_d mesons are identified through the decay chain $B^0_d \to D^{*-}X$, $D^{*-} \to \overline{D}^0\pi^-$, where the $\overline{D}^0$ then decays into one of $K^-\pi^+$, $K^-\pi^+\pi^0$, or $K^-\pi^+\pi^+\pi^-$. Requirements similar to those of Ref. [1] are placed on the decay products of the D^0 to reduce combinatorial backgrounds. Further requirements are imposed, as discussed below, on all decay channels as part of the separate lepton and jet charge subsample selections. The final sample consists of 840 D^*-lepton events and 1555 D^*-jet-charge events. These are associated with a combinatorial background of 565 and 1096 events respectively, of which over 90% is in the $K^-\pi^+\pi^0$ and $K^-\pi^+\pi^+\pi^-$samples. The sample is assumed to consist of D^* from B^0_d and B^+ decays, from direct charm production, and from combinatorial background.

3.2 Initial state determination

The determination of the initial state is performed primarily using information from the hemisphere of the event opposite to that of the D^*. The preferred method, because of its lower mistag rate and higher b purity, is to use the lepton coming from the semileptonic decay of a b hadron. Otherwise the event sample is enriched by the use of the impact parameter tag of Ref. [11]. In this case, the probability for the hemisphere opposite to the D^* to originate from uds production is required to be less than 0.005. This gives a charm fraction close to that expected in the lepton subsample (Table 1).

Electrons and muons are selected using standard ALEPH lepton identification techniques [7]. The lepton is required to have a momentum $p > 3.0\,\mathrm{GeV}/c$ and a momentum transverse to its jet $p_\mathrm{T} > 0.75\,\mathrm{GeV}/c$, where this is calculated with the lepton excluded from its jet. These requirements control both the fraction of $b \to c \to \ell$ cascade decays (which have the opposite sign), and the primary charm fraction in the sample.

For events without a valid lepton candidate, information from charged tracks in both hemispheres of the event is used. In the hemisphere opposite to the D^* a momentum

[2] Unless otherwise specified, references to a decay process are taken to include its charge conjugate, and D^* refers to the $D^{*-}(2010)$ state.

Parameter	Measured value	Expected value
Δm_d (ps^{-1})	0.482 ± 0.044	–
Charm fraction (lepton sample)	0.10 ± 0.02	0.09
Charm fraction (jet charge sample)	0.12 ± 0.03	0.08
B^0_d Mistag rate (lepton sample)	0.21 ± 0.04	0.24
B^0_d Mistag rate (jet charge sample)	0.24 ± 0.03	0.28

Table 1: Results of the D^* fit. The last column contains the expected values (where relevant), as extracted from Monte Carlo studies.

weighted "jet" charge is calculated:

$$Q_{\rm H} = \frac{\sum_i |\vec{p_i} \cdot \vec{e}_{\rm T}|^\kappa \cdot q_i}{\sum_i |\vec{p_i} \cdot \vec{e}_{\rm T}|^\kappa}, \tag{2}$$

where $|\vec{p_i} \cdot \vec{e}_{\rm T}|$ is the momentum component of particle i along the thrust axis, q_i is its charge, and the hemispheres are defined according to the thrust axis. A value for κ of 0.5 has been shown [10] to give optimal charge separation in b jets. In the D^* hemisphere the sum of the charges Σq is calculated, which reflects the charge of the remaining fragmentation tracks of the event, and hence that of the initial charge of the b quark (since the sum of the charges of the B^0_d tracks are zero independently of whether it has mixed). A linear combination of opposite- and same-hemisphere charges, $\Delta Q \equiv Q_{\rm H} - 0.08 \cdot \Sigma q$, is used to sign the initial charge of the B^0_d (the relative weights are optimized using Monte Carlo studies). Furthermore, to maximize the sensitivity, events with $|\Delta Q| < 0.10$ are rejected, removing 30% of the events. The mistag rate is somewhat higher than that in events using a lepton tag (Table 1), but this is compensated by the larger size of the event sample.

3.3 The charge correlation function

Decay length distributions for like- and unlike-sign events are each fitted, using an unbinned maximum likelihood method, to a function that contains, as discussed in Ref. [1], terms for the various components of the sample, convoluted with momentum distribution and decay length resolution functions. The B^0_d component consists of two exponential decay terms (one for the B^0_d and one for the D^0, where the D^0 decay length convolution has little effect upon the visibility of the oscillation), modulated by a time-dependent oscillation function. The background components for direct charm and charged b hadrons are parametrized by exponential decay functions. The charm fraction is fitted, in the $K^-\pi^+$ channel, with one parameter each for the lepton and jet charge subsamples; the relative abundances for the other D^0 decay modes are fixed in proportion to the ratio of the respective products of branching ratio and reconstruction efficiency as determined from Monte Carlo. The fraction of $B^+ \to D^{*-}$ decays and the mistag rate for these decays are fixed to values determined using Monte Carlo simulations. The decay length dependence of the combinatorial background, its charge correlation, as well as the number of background events, are taken from fits to the sidebands of the D^0 mass and the $D^* - D^0$ mass difference distributions.

The following parameters are fitted: Δm_d and, separately for the lepton and jet-charge samples, the mistag probability and the charm fraction. The total number of events is allowed to vary within a Gaussian constraint that reflects the number observed. The data

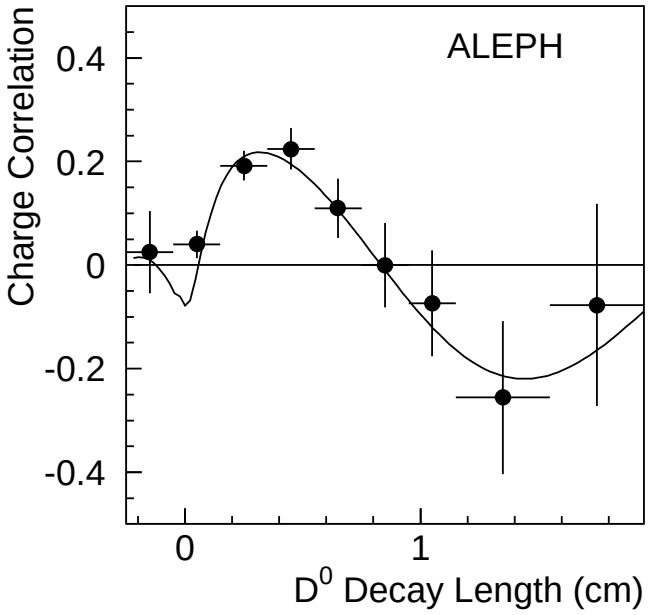

Figure 1: Charge correlation as a function of the reconstructed D^0 decay length, with superimposed fit.

and fit are presented in Fig. 1, in terms of the charge correlation

$$\frac{N^{\rm ss} - N^{\rm os}}{N^{\rm ss} + N^{\rm os}} \tag{3}$$

as a function of the decay length, where $N^{\rm ss}$ is the number of same-sign events, and $N^{\rm os}$ the number of opposite-sign events. The power of this method lies principally in the region of zero crossing in the charge correlation function, where most backgrounds are small, and where there are still enough events to provide sensitivity.

3.4 Results and systematic studies

The results obtained from the fit are summarized in Table 1. The fitted and expected values are consistent. Several sources of systematic uncertainty are explored, and their effects are summarized in Table 2.

The largest component of the systematic error comes from the uncertainty affecting the B^+ contamination of the sample. The fraction of B^+ events is set to a central value of 0.17 obtained from Monte Carlo studies, and varied by ± 0.08 to account for the lack of knowledge of B^0_d and B^+ decays via D^{**} states. This fraction and error have been extracted in a manner similar to that discussed in Ref. [12], and the values are comparable to those found there. A fit with the B^+ fraction free gives a value of 0.04 ± 0.27, and yields $\Delta m_d = 0.453 \pm 0.059\,{\rm ps}^{-1}$.

The mistag rate of the B^+ component may be affected by the poorly understood rate of D^* production from the virtual W; its central value is taken from the Monte Carlo (0.38 for the lepton sample and 0.35 for the jet charge sample), and varied by 50% to provide a systematic error.

Uncertainties on the lifetimes of charged and neutral B mesons have a small effect. The values are taken from Ref. [13]. The errors are determined by first varying τ_{B_d}, while holding τ_{B_d}/τ_{B^+} constant. Then τ_{B^+} is varied while holding τ_{B_d} at its nominal value. The D^0 lifetime [14] is varied by its measurement uncertainty.

Parameter	Variation	$\sigma_{\rm sys}$ ($\rm ps^{-1}$)
B^+ fraction	0.17 ± 0.08	± 0.018
B^+ mistag rate	$\pm 50\%$	± 0.010
τ_{B_d}	1.564 ± 0.048 ps	∓ 0.002
τ_{B^+}	1.617 ± 0.046 ps	± 0.002
τ_{D^0}	0.415 ± 0.004 ps	± 0.002
$Q^{\rm bkg}$	sideband $\pm 1\sigma$	± 0.006
Charm acceptance	$\pm 10\%$	± 0.006
Resolution function	MC parametrization	-0.006
b fragmentation $\langle x_b \rangle$	0.714 ± 0.012	± 0.007
D^0 momentum	$\pm 5\%$	± 0.003
Total		± 0.024

Table 2: Sources and values of systematic errors ($\sigma_{\rm sys}$) on Δm_d for the D^* method. The parameters for which no central value is listed are discussed in the text. The symbol $\mp$ is used for those variables which when increased lead to a decrease in the fitted value of Δm_d.

As a consistency check, the B^0_d lifetime has been fitted using this data sample, with a resulting value of $\tau_{B_d} = 1.497 \pm 0.077$ ps (where the error is statistical only), consistent with the world average.

The direct charm fraction is fitted in the $K^-\pi^+$ mode with one parameter for each of the lepton and jet-charge samples. For the other two decay modes, the fraction is obtained by multiplying this fit parameter by the ratio of the product of efficiencies and branching ratios. A systematic error is assigned by varying each of these acceptance ratios by its Monte Carlo statistical uncertainty (approximately 10%).

In the fit the resolution function is determined from the data using events where the probability that the event comes from light quark production is high. This probability is calculated using the charged track impact parameters in one hemisphere according to the method of Ref. [11]. The resolution is then determined using tracks in the other hemisphere. For the assignment of a systematic error, the fit is repeated using the resolution function calculated from the Monte Carlo simulation.

The combinatorial background charge correlation $Q^{\rm bkg}$ is determined from fits to the sidebands of the D^0 mass and the $D^* - D^0$ mass difference distributions. The quoted error corresponds to a variation of the charge correlation by the uncertainty of these fits.

The D^0 and B^0_d momentum spectra used in the fit are determined from Monte Carlo studies. The mean of the measured D^0 spectrum differs by 5% from that in the Monte Carlo, and the assigned error comes from reweighting the values in the fit by this amount. The uncertainty on the b hadron momentum spectrum is taken into account by reweighting it according to the variation of the fragmentation parameter $\langle x_b \rangle$ used in the Monte Carlo, within its error [8].

The fit is insensitive to B^0_s mixing, as the number of $B^0_s \to D^{*-} X$ events in the sample is expected to be small, due to the relatively low rate of B^0_s production and to the small B^0_s branching ratio to D^*.

The result for Δm_d is then

$$0.482 \pm 0.044 \pm 0.024 \ \rm ps^{-1},$$

where the first error is statistical and the second systematic. This value is consistent with the previously published result [1].

4 Lepton-jet method

If a b hadron decays to a lepton (after having possibly undergone oscillation), the charge of the decaying quark and the decay time itself are related, respectively, to the lepton charge and to the distance between the primary event vertex and the decay vertex from which the lepton originates. The charge of that same b quark at production time is extracted from the jet charge in the hemisphere opposite to the lepton.

The jet charge is defined as the momentum-weighted charge average over all charged particles in that hemisphere according to Eq. 2. The basic quantity measured is the time dependence of the lepton-signed jet charge $Q_{\ell \mathrm{H}}(t) = -\langle q_\ell \times Q_{\mathrm{H}} \rangle$, defined as the average, in a time bin and over the sample of leptons, of the product of the lepton charge and the jet charge in the hemisphere opposite to the lepton. For a pure sample of $b \to \ell$ decays the quantity $Q_{\ell \mathrm{H}}$ is positive on average, when the lepton originates from a b hadron that did not mix, and negative, if the lepton is produced by a B^0 that oscillated to its antiparticle. $Q_{\ell \mathrm{H}}(t)$ is simply related to the oscillation frequencies:

$$\begin{aligned} Q_{\ell \mathrm{H}}(t) &= \langle Q_{\mathrm{H}} \times \mathrm{sign}(q^{\mathrm{opp}}_{\mathrm{quark}}) \rangle \times \langle q_\ell(t) \times \mathrm{sign}(q^{\mathrm{same}}_{\mathrm{quark}}) \rangle \\ &= Q_b \times \left(1 - \tilde{f}_d - \tilde{f}_s \; + \; \tilde{f}_d \cos(\Delta m_d t) \; + \; \tilde{f}_s \cos(\Delta m_s t) \right) . \end{aligned} \tag{4}$$

In this equation, $q^{\mathrm{opp}}_{\mathrm{quark}}$ is the charge of the primary quark in the hemisphere opposite to the lepton, and $q^{\mathrm{same}}_{\mathrm{quark}}$ that of the primary quark in the lepton hemisphere. The notation implicitly ignores correlations between the lepton and the opposite-hemisphere charge; these have been verified in the simulation to be completely negligible. Rewriting the above equation in terms of measurable quantities, the first factor, Q_b, is the average quark-signed charge of a b jet. The second factor is the average lepton charge. It exhibits a time-independent contribution from charged B mesons and b baryons, and oscillation terms (corresponding to B^0_d and B^0_s mesons); these are proportional to $\tilde{f}_d$ and $\tilde{f}_s$, the fractions of leptons originating from primary $b \to \ell$ decays of B^0_d and B^0_s mesons respectively. This simplified formula must be generalized (Section 4.3) to take into account $b \to c \to \ell$ decays, as well as charm and other backgrounds.

4.1 Event selection and sample composition

In addition to the event selection mentioned in Section 2, the events must satisfy $|\cos \theta_{\mathrm{thrust}}| < 0.85$, and contain at least two jets defined using the JADE clustering algorithm [15] with a minimum jet separation of $(6\ \mathrm{GeV}/E_{\mathrm{cm}})^2$.

In order to ensure that the lepton-jet and dilepton results remain statistically independent, all events appearing at the final stage of the dilepton selection (Section 5) are explicitly excluded from this analysis. Similarly, overlap with the D^* method was checked: less than 1% of the lepton-jet events appear in the sample described in Section 3, and their impact on the lepton-jet Δm_d measurement is negligible.

To enrich the sample in $b \to \ell$ decays, the remaining events are required to contain at least one electron or muon, identified on the basis of the standard ALEPH lepton identification criteria [7], and satisfying $p > 3\ \mathrm{GeV}/c$ and $p_{\mathrm{T}} > 1.25\ \mathrm{GeV}/c$. This lepton is required to have at least one vertex detector hit in each of the $r\phi$ and z projections. The hemisphere opposite to the lepton is treated in an inclusive fashion; in particular, if an event contains several leptons passing all the cuts, all "lepton–opposite-hemisphere" pairs (hereafter called "lepton-jet" pairs for the sake of brevity) are considered independently in the analysis. A total of 63 131 leptons passing the above criteria, and containing a valid secondary vertex as defined in Section 4.2, are found in 62 320 events.

This sample consists of primary b semileptonic decays ($b \to \ell$), cascade decays ($b \to c \to \ell$) with fraction f_{bc}, charm semileptonic decays ($c \to \ell$) with fraction f_c, and other backgrounds (non-prompt leptons and misidentified hadrons) with fraction $f_{\rm bkg}$. These source fractions, listed in Table 3, are determined by the method reported in Ref. [8], but with the *uds* component of the background increased to take into account the discrepancies observed between data and Monte Carlo [16]. The uncertainties inherent to this procedure are included in the systematic error ($\pm$ 25%) on the total background fraction, which is chosen to be comparable to the overall correction (+22%).

4.2 Proper time reconstruction

The proper time is reconstructed as the product of the flight distance d and the boost factor m_B/p_Bc, where m_B and p_B are the mass and momentum of the b hadron. The flight distance measurement and the momentum reconstruction are optimized for the $b \to \ell$ topology; the performance is different for $b \to c \to \ell$, $c \to \ell$ and background leptons. This is taken into account in the modelling of the measured time distribution by the use of different efficiency and resolution functions for each lepton source.

After dividing the event into two hemispheres perpendicular to the thrust axis, the primary vertex and a decay (charm-like) vertex are reconstructed using an inclusive vertexing technique [2]. Charged tracks (excluding the lepton) that are consistent with the reconstructed charm vertex within 1.4 standard deviations, and satisfy $p > 1.5\,{\rm GeV}/c$, are then fitted to a common vertex; the sum of their momenta is used to define the direction of the charm candidate. If only one such track is found, it is taken as the charm candidate; if no charm track is found, the lepton is rejected. The charm track is finally vertexed with the lepton to give the b hadron decay point. A cut of $\chi^2/{\rm dof} < 25/1$ is applied to the b decay vertex. The b hadron flight distance is taken as the distance in space between the primary and b decay vertices, projected onto the axis of the jet to which the lepton belongs. The decay length resolution for $b \to \ell$ decays, as determined from the Monte Carlo, exhibits on the average a core with a $\sigma \approx 270\,\mu$m containing 62% of the events, and a tail with $\sigma \approx 1.1$ mm. This resolution depends on the b hadron flight distance itself, due to primary tracks being misassigned to the secondary vertex and pulling the latter back towards the primary. For similar reasons, the efficiency for reconstructing a secondary vertex decreases with increasing b hadron flight distance; it is extracted from the simulation and checked by measuring the b hadron lifetime in the data.

The b hadron momentum is estimated using the sum of the lepton energy, the charged energies at the charm vertex, the missing energy in the hemisphere, and a neutral energy contribution; the last of these depends on the observed neutral electromagnetic energy in the jet of the lepton in a manner determined from the simulation, and accounts for the contribution of the neutral hadronic energy and for jet clustering errors. The resolution on the boost factor is approximately 20% RMS for $b \to \ell$ decays.

The measured proper-time distribution of the lepton-jet sample is the superposition of the distributions corresponding to the subprocesses listed in Section 4.1. In order to predict the measured time distribution corresponding to a given set of b hadron lifetimes, the generated proper time distribution for $b \to \ell$ decays is first weighted by the distance-dependent efficiency function. It is then convoluted with the resolution function, parametrized directly in terms of proper time (as a sum of Gaussians) and extracted from the simulation in slices of true proper time. The decay length resolution is partially checked on data by selecting fake leptons, i.e. charged tracks that satisfy the same geometrical and kinematical cuts as the leptons but are required to fail the lepton

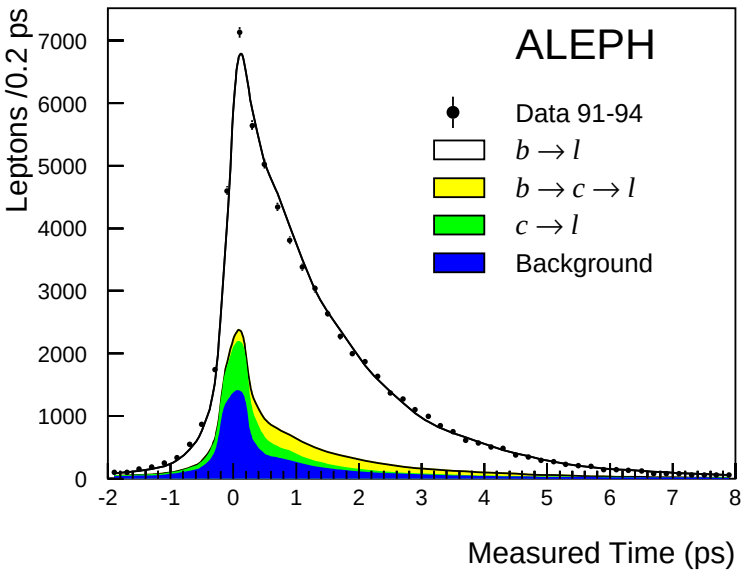

Figure 2: Measured time distribution in the lepton-jet analysis. The time distributions corresponding to the different lepton sources are shown in shades of grey: background leptons, charm, cascade leptons, and (unshaded) primary b's, from bottom to top.

identification criteria. As observed elsewhere [2, 17], the comparison between data and Monte Carlo of the flight distance distributions for fake leptons in uds-enriched events suggests that the resolution in the Monte Carlo should be widened when analyzing data. A global corrective scale factor 1.07 ± 0.07 is applied to the width of the time resolution functions, in all slices of proper time.

A similar procedure is followed for cascade leptons ($b \to c \to \ell$), with appropriate efficiency and resolution functions. For charm and backgrounds, the predictions for the reconstructed time distributions are taken directly from the Monte Carlo.

These four underlying distributions are then combined in proportion to their source fractions, and fitted to the proper-time distribution measured in the data to extract the average b lifetime. Applying this procedure to a Monte Carlo sample generated with $\tau_b = 1.5\,\mathrm{ps}$, the fit returns $\tau_b = 1.496 \pm 0.012\,\mathrm{ps}$, with $\chi^2/\mathrm{dof} = 59/49$. Repeating the procedure for the data, one obtains $\tau_b = 1.530 \pm 0.010\,\mathrm{ps}$ (the error is statistical only), consistent with the world average. But the fit is poor (Fig. 2): $\chi^2/\mathrm{dof} = 244/49$, with the dominant distortion arising for absolute values of proper time less than 1.0 ps, as also noted in Ref. [17]. A detailed study of the possible source of this discrepancy suggests it may be due to differences between data and Monte Carlo in the rate of track misassignments from the primary to the charm vertex. It will be shown below that the Δm_d measurement is stable with respect to a cut applied to the measured time which eliminates part or all of the region of poor agreement.

4.3 Δm_d measurement

The measured lepton-signed jet charge for a pure sample of $b \to \ell$ decays depends on the true time-dependent lepton-signed jet charge, which contains the Δm_d and Δm_s information (Eq. 4). This distribution is weighted by the true parent lifetime distributions and by the vertexing efficiency for $b \to \ell$ decays, and convoluted with the resolution in

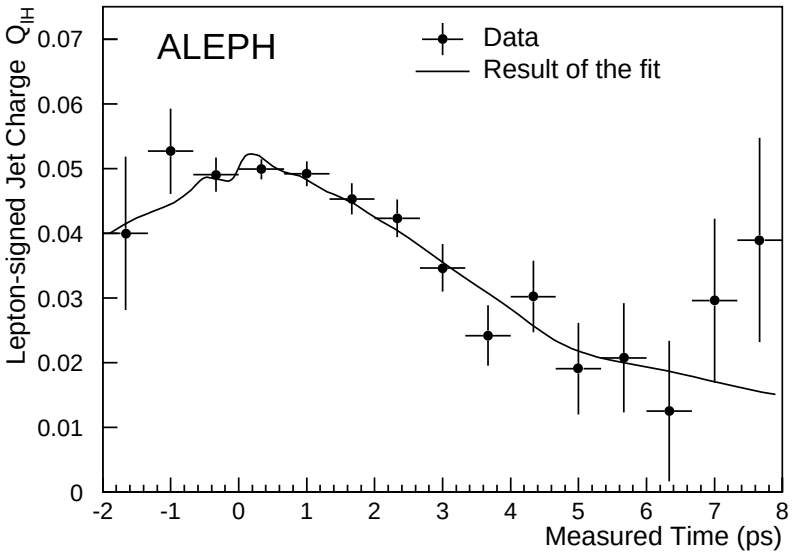

Figure 3: Lepton-signed jet charge vs. proper time (the binning used in the fit is finer, 0.2 ps, so as not to affect the result).

proper time. Similar considerations apply to the cascade contribution, which also carries mixing information. Account must also be taken of charm leptonic decays, and of non-prompt leptons and misidentified hadrons. The measured lepton-signed jet charge for the whole data sample is then the sum of the lepton-signed charges for each source, weighted by the time-dependent fraction each source contributes.

A multiparameter fit is performed simultaneously to the inclusive proper time distribution (Fig. 2) and to the time-dependence of the measured lepton-signed jet charge (Fig. 3). The B^0_d oscillation frequency Δm_d and the average b jet charge Q_b are left free in the fit.

The exclusive b baryon and meson lifetimes, and the production fractions f_{Λ_b} and f_s of b baryons and B^0_s mesons, are allowed to vary within Gaussian constraints (Table 3) taken from Refs. [13, 18]. The B^0_d and B^+ production fractions are expressed in terms of the baryon and B^0_s fractions,

$$f_d = f_{B^+} = 0.5 \times (1 - f_s - f_{\Lambda_b}). \tag{5}$$

The b hadron fractions in the lepton sample, $\tilde{f}_d$ and $\tilde{f}_s$, are then calculated by weighting the fractions at production by the corresponding semileptonic branching ratios, which are assumed to be proportional to the corresponding lifetimes. An additional constraint is imposed on the multiparameter fit, requiring that the production-weighted average of exclusive lifetimes be consistent with the world-average measurement of the inclusive b lifetime τ_b [13]:

$$f_d\ (\tau_{B_d} + \tau_{B^+})\ +\ f_s\ \tau_{B_s}\ +\ f_{\Lambda_b}\ \tau_{\Lambda_b}\ =\ \tau_b \pm \sigma_{\tau_b}. \tag{6}$$

The background and charm charges $Q^{\ell\mathrm{H}}_{\mathrm{bkg}}$ and $Q^{\ell\mathrm{H}}_c$ are allowed to vary within Gaussian constraints, determined as follows. The value and the time-dependence of the background charge are taken from the Monte Carlo; the allowed range of variation of the charge is equal to the statistical error in the simulation ($\pm 50\%$). The lepton-signed charm charge is time-independent, as it relies only on the hemisphere opposite to the lepton. An inclusive

Parameter	Variation	Fitted value	$\sigma_{\rm sys}$ ($\rm ps^{-1}$)
τ_{B_d}	1.564 ± 0.048 ps	1.550 ± 0.037 ps	∓ 0.010
τ_{B_s}	1.551 ± 0.106 ps	1.537 ± 0.090 ps	∓ 0.005
τ_{Λ_b}	1.179 ± 0.072 ps	1.188 ± 0.069 ps	± 0.006
τ_{B^+}	1.617 ± 0.046 ps	1.608 ± 0.035 ps	± 0.014
f_{Λ_b}	0.128 ± 0.039	0.127 ± 0.035	± 0.005
f_s	0.102 ± 0.016	0.102 ± 0.016	∓ 0.001
$Q_c^{\ell \rm H}$	0.093 ± 0.012	0.090 ± 0.011	∓ 0.007
$Q_{\rm bkg}^{\ell \rm H}$	0.019 ± 0.008	0.018 ± 0.007	∓ 0.004
τ_b	1.563 ± 0.020 ps	–	∓ 0.001
f_{bc}	0.065 ± 0.009	–	∓ 0.012
f_c	0.057 ± 0.006	–	∓ 0.002
$f_{\rm bkg}$	0.113 ± 0.025	–	± 0.008
$\tilde{f}_d^{bc} = \tilde{f}_d$, $\tilde{f}_s^{bc} = \tilde{f}_s$		–	-0.006
Resolution	1.07 ± 0.07	–	± 0.009
Δm_s	$\infty \rightarrow 6\,\rm ps^{-1}$	–	-0.002
Other		–	± 0.005
Total			± 0.028

Table 3: Contributions to the systematic error on Δm_d in the lepton-jet analysis. The second column shows the world-average values with their errors, which are used as Gaussian constraints, for those parameters which are fitted together with Δm_d and Q_b; the third column displays the result of the fit. The top half of the table corresponds to the constrained quantities, and the bottom half to the "fixed" parameters. The central value and range of variation of the fixed parameters are also listed. The fourth column displays the contribution of each source to the systematic error on Δm_d.

value has been measured by ALEPH [19]. In order to account for the exclusion of dilepton events, this measured value is corrected by a scale factor extracted from the simulation; the allowed range of variation is equal to the published experimental error.

The source fractions are not fitted but kept fixed to the central values listed in Table 3. The value of Δm_s is kept fixed to infinity; the possibility of non-maximal B_s^0 mixing is taken into account in the systematic error.

The fit to the 1991–94 ALEPH data yields $\Delta m_d = 0.396 \pm 0.050\,\rm ps^{-1}$ and $Q_b = 0.0668 \pm 0.0028$. The fit results for the other parameters are compared to their input constraints in Table 3.

Consistency of the results between electrons and muons, between different data-taking periods, and for different choices of the jet charge parameter κ, was extensively checked [20]. In addition, the procedure described above has been applied to fully simulated Monte Carlo data; all fitted parameters are found to be consistent with the corresponding generated values.

4.4 Systematic errors

The error on Δm_d quoted above includes both the statistical error, and the systematic error associated with other fitted parameters. In order to evaluate the systematic error associated with each fitted parameter separately, the fitting procedure above is repeated,

varying the central value of each constraint in turn by one standard deviation (Table 3). The purely statistical error on Δm_d is then estimated by subtracting in quadrature, from the total error of the multiparameter fit, the quadratic sum of the systematic errors associated with the fitted parameters.

Systematic errors associated with the "fixed" parameters are estimated by a similar procedure, where each parameter in the bottom half of Table 3 is varied by one standard deviation, and the fitting procedure repeated.

The final lepton-jet result is then

$$\Delta m_d = 0.396 \ \pm 0.045 \ \pm 0.028 \ \mathrm{ps}^{-1},$$

where the first error is statistical and the second systematic.

The largest systematic errors arise from the lifetimes τ_{B_d} and τ_{B^+}. An increase in τ_{B_d} implies a larger fraction of B_d^0 at long proper times. As these "extra" B_d^0's would lie near the minimum of the cosine curve (half a period), their lepton-signed charge would pull down the average; as this is however constrained by the data, the fit compensates by reducing Δm_d. A decrease in τ_{B^+} has the same effect because it decreases the fraction of non-oscillating b hadrons at long proper time. Decreasing τ_{Λ_b} has a similar but reduced effect due to the low fraction of b baryons. The B_s^0 lifetime also contributes to the error because, in the limit of infinite Δm_s, the average charge due to B_s^0-induced leptons is zero. When τ_{B_s} increases, the B_s^0 population at large times increases, the mean charge decreases, and the effect is similar to that of τ_{B_d}. All these effects occur because there are relatively few events with proper time greater than a half period, thereby inducing a correlation between Q_b and Δm_d [20].

The next largest error is associated with the cascade fraction f_{bc}, which is again correlated with the amplitude of the oscillation: the larger the assumed cascade fraction, the smaller the predicted amplitude, and the smaller the fitted Δm_d.

Increasing the baryon fraction leads to two anticorrelated effects of comparable magnitude. On the one hand, the B_d^0 fraction decreases. The fewer B_d^0 the sample is assumed to contain, the weaker the expected time dependence of $Q_{\ell \mathrm{H}}$; as the latter is constrained by the data, Δm_d has to increase to balance the assumed decrease of $\tilde{f}_d$. On the other hand, as the Λ_b^0 lifetime is small compared to that of other b hadrons, increasing f_{Λ_b} decreases the average b lifetime, while the B_d^0 lifetime is unchanged. Again, this increases the assumed B_d^0 fraction at long proper time, and the fitted value of Δm_d has to decrease.

The systematic error associated with the B_s^0 fraction is very small due to two other anticorrelated effects of almost equal magnitude. Increasing f_s increases the B_s^0 fraction at long proper time, and as their average charge is zero, Δm_d decreases (as was the case for τ_{B_s}). On the other hand, the B_d^0 fraction decreases, and so Δm_d tends to increase, compensating the first effect.

The error associated with the time resolution is estimated by varying the resolution-widening correction discussed in Section 4.2. As is apparent in Fig. 2, there remains a systematic disagreement between the measured time distribution in data compared to Monte Carlo. To ascertain the potential impact on Δm_d, the measurement was repeated by increasing the minimum proper time considered in the fit, progressively excluding the region of poor agreement. The measured value of Δm_d deviates by no more than 0.8 standard deviations from the original result, in a manner consistent with statistical fluctuations.

The proportions of B_d^0 and B_s^0 mesons in cascade decays, $\tilde{f}_d^{bc}$ and $\tilde{f}_s^{bc}$, respectively, are different from the proportions in primary b semileptonic decays, because of different

decay channels and branching ratios. As the latter are poorly known, the error quoted corresponds to setting the B_d^0 fractions in primary and cascade semileptonic decays arbitrarily equal to each other (and similarly for the B_s^0).

The error due to Δm_s is evaluated by refitting Δm_d with $\Delta m_s = 6$ ps^{-1}, which corresponds to the lower limit from Ref. [18]. Finally, the error labelled "Other" accounts for the slight difference between data and Monte Carlo in the b hadron energy distributions, and for the uncertainty affecting the time dependence of the vertexing efficiency.

5 Dilepton method

In this section the published dilepton analysis [2] is updated to include the data taken in 1993–1994. The method used is essentially unchanged; a summary is given here, but the original publication should be referred to for details.

The particle/antiparticle state of the B^0 is determined at both its production and decay time using dilepton events in hadronic Z decays. The two leptons (electrons and/or muons) are required to be separated by more than 90^0, and to have high transverse momentum $p_{\rm T}$ with respect to their associated jets, giving a high probability that they originate from semileptonic b decays. The sign of the lepton charge tags the state of the b hadron, and if either of the b hadrons is a B^0 that oscillates to its antiparticle a like-signed dilepton event will result. The fraction of dilepton events in which the leptons have like sign is then studied as a function of the proper time of the B^0 decay. The measurement of proper time is achieved by measuring the decay length of the b hadron, using the lepton and other charged tracks in a vertexing technique closely related to that described in Section 4. The decay length is converted to proper time by estimating the momentum of the b hadron from the momenta of its decay products, using the missing energy of the hemisphere to account for the neutrino from the semileptonic decay. Each dilepton event can provide up to two measurements of the decay time, and the distribution of reconstructed times of unlike- and like-sign events is fitted using a maximum-likelihood technique to extract the oscillation parameters. Since B_d^0 and B_s^0 mesons both contribute to dilepton events, the measurement is sensitive to Δm_d and Δm_s. For the measurement of Δm_d described here, maximal B_s^0 oscillation is assumed (i.e. $\Delta m_s \to \infty$); the effect of a lower value of Δm_s is included as a systematic error.

The technique of reconstructing the proper time is unchanged from Ref. [2]. Dilepton events are selected requiring $p_{\rm T} > 1.25\,{\rm GeV}/c$ for both leptons, with at least one lepton providing a measurement of proper time; there are 5957 such events, and a total of 9710 leptons in the sample with measured proper time. Forty of these events are common to the D^* analysis described in Section 3, and are removed to ensure statistical independence of the two results. The proper-time resolution is determined from Monte Carlo simulation, with a scale factor of 1.07 ± 0.07 applied to account for the slightly poorer decay-length resolution observed for the data in control samples; the uncertainty on this factor is used below in systematic error studies. The proper-time distributions expected for each of the various possible sources of leptons are determined. A small excess of events is observed at small proper time, as discussed in Section 4.2. Here, this effect is corrected for by including a component $f_0 = (3 \pm 3)\%$ of decays which are assigned the resolution function for their proper time distribution, as if they had zero lifetime.

The B^0 oscillation should be visible as a sinusoidal behaviour of the fraction of dilepton events with like-signed leptons, as a function of proper time (proportional to $1 - \cos\,\Delta m\, t$,

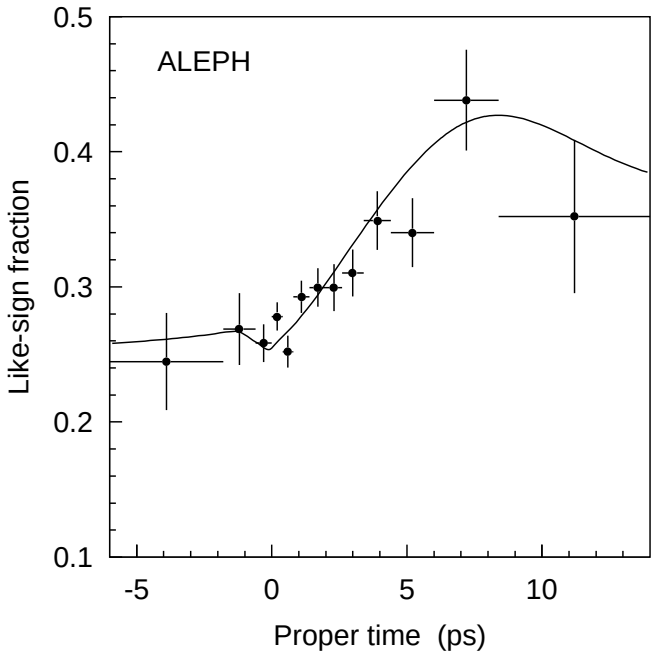

Figure 4: The like-sign fraction for dileptons, as a function of reconstructed proper time, with the result of the fit for Δm_d shown superimposed, assuming maximal B_s^0 mixing.

but damped by the resolution). This "like-sign fraction" is shown in Fig. 4. The fitting technique is similar to that described in Ref. [2], slightly modified to be compatible with that of the lepton-jet charge analysis of Section 4: Δm_d is left as a free parameter, and five other parameters are allowed to vary in the fit within constraints. These are the inclusive b lifetime τ_b, the B_d^0 and B_s^0 lifetimes, and the B_s^0 and b baryon production fractions f_s and f_{Λ_b}. Gaussian constraints are applied to these parameters according to their world-average values and errors [13, 18], listed in Table 4.

The result of the fit is shown in Fig. 4, and gives $\Delta m_d = 0.426 \pm 0.051$ ps^{-1}; the fitted values of the other parameters are listed in Table 4. The systematic error on Δm_d from these parameters is estimated by varying the central value of each constraint by $\pm 1\sigma$ in turn, and refitting for Δm_d. The change in Δm_d is taken as the contribution to the systematic error and is listed in Table 4. The statistical error on Δm_d (0.039 ps^{-1}) is then determined by requiring that its sum in quadrature with these five systematic error contributions gives the total error on the original fit (0.051 ps^{-1}). Other contributions to the systematic error are determined by varying the values of inputs to the fit as listed in Table 4, with the results shown. The various contributions are added in quadrature, leading to a final result of

$$\Delta m_d = 0.426 \pm 0.039 \pm 0.052 \text{ ps}^{-1},$$

where the first error is statistical and the second systematic. This value is consistent with the previous result [2]; the statistical error is reduced as expected for the increased data sample, and the systematic error is also smaller due to the improved constraints on the other variables in the fit.

Parameter	Variation	Fitted value	$\sigma_{\rm sys}$ ($\rm ps^{-1}$)
τ_{B_d}	1.564 ± 0.048 ps	1.525 ± 0.041 ps	∓ 0.014
τ_{B_s}	1.551 ± 0.106 ps	1.539 ± 0.099 ps	∓ 0.016
τ_b	1.563 ± 0.020 ps	1.538 ± 0.014 ps	± 0.004
f_{Λ_b}	0.128 ± 0.039	0.138 ± 0.039	± 0.014
f_s	0.102 ± 0.016	0.123 ± 0.012	∓ 0.021
f_{bc}	0.070 ± 0.010	–	∓ 0.033
f_c	0.005 ± 0.002	–	± 0.001
$f_{\rm bkg}$	0.024 ± 0.012	–	∓ 0.013
f_0	0.03 ± 0.03	–	± 0.003
Resolution	1.07 ± 0.07	–	∓ 0.004
Δm_s	$\infty \rightarrow 6\ \rm ps^{-1}$	–	$+0.007$
Other		–	± 0.017
Total			± 0.052

Table 4: Contributions to the systematic error on Δm_d in the dilepton method. The entry marked "Other" includes the effect of varying the mistag fractions and proper-time distribution parametrizations for the background sources of leptons, within their uncertainties.

6 Combination of Δm_d results

The D^*, dilepton and lepton-jet samples were selected so as to remain statistically independent, as discussed in Sections 4.1 and 5.

The systematic uncertainties affecting the D^* measurement are almost independent from those affecting the dilepton and lepton-jet results, as seen by comparing the sources and magnitudes of the errors listed in Tables 2, 3, and 4. However, the dilepton and lepton-jet-charge methods share correlated sources of systematics, such as the uncertainties on world-averaged lifetime measurements. Such correlations must be handled differently depending on how the physical quantity considered is treated in the dilepton and lepton-jet analyses:

- some quantities, such as the B^0_d lifetime, are allowed to vary (under external constraint) together with Δm_d in a multiparameter fit. Some appear only in the dilepton analysis, some in the lepton-jet analysis only, and some are common to both analyses.

- Other quantities, such as the cascade fraction f_{bc}, are fixed to a value determined *a priori* (in this case from Monte Carlo simulation) when the central values of Δm_d are extracted from the dilepton and lepton-jet fits. These parameters are then varied, one at a time, by plus or minus one standard deviation, and the Δm_d fits repeated, in order to assess the systematic uncertainty such parameters contribute to the Δm_d measurements. Again, some appear in only one analysis, while others are common to both.

Combining the results of Sections 4.4 and 5 in a global fit that takes the above correlations into account, $\Delta m_d = 0.401 \pm 0.044\ \rm ps^{-1}$ is obtained. The systematic errors affecting this combined result for the dilepton and lepton-jet analyses are listed in Table 5. As expected, the global error is slightly higher than what would have been obtained by

Parameter	$\sigma_{\rm sys}$ ($\rm ps^{-1}$)
τ_{B_d}	$\mp$ 0.008
τ_{B_s}	$\mp$ 0.006
τ_{Λ_b}	$\pm$ 0.006
τ_{B^+}	$\pm$ 0.011
τ_b	$\pm$ 0.003
f_{Λ_b}	$\pm$ 0.005
f_s	$\mp$ 0.005
Q_c	$\mp$ 0.005
$Q_{\rm bkg}$	$\mp$ 0.002
f_{bc}	$\mp$ 0.021
$f_{\rm bkg}$	$\mp$ 0.002
Resolution	$\pm$ 0.004
Δm_s	+ 0.004
Uncorrelated dilepton syst.	$\pm$ 0.007
Uncorrelated ℓ-jet syst.	$\pm$ 0.005
Total	$\pm$ 0.030

Table 5: Systematic errors on Δm_d for the combined dilepton + lepton-jet result.

naively assuming the systematics were independent (0.407 ± 0.041 $\rm ps^{-1}$). Combining the above measurement with the D^* result (from Section 3), the final ALEPH result is obtained: $\Delta m_d = 0.436 \pm 0.033$ $\rm ps^{-1}$.

7 Conclusions

Three analyses of B^0_d–$\overline{B}^0_d$ mixing are presented. Using the data collected by ALEPH in 1991 to 1994, the update of the D^* method gives $\Delta m_d = 0.482 \pm 0.044 \pm 0.024\,\rm ps^{-1}$; the analysis of an inclusive sample of lepton-jet events yields $\Delta m_d = 0.396 \pm 0.045 \pm 0.028\,\rm ps^{-1}$; and the update of the dilepton analysis gives $\Delta m_d = 0.426 \pm 0.039 \pm 0.052\,\rm ps^{-1}$. These event samples are selected so as to eliminate statistical overlap between them. After accounting for common systematic uncertainties, the final ALEPH result is

$$\Delta m_d = 0.436 \pm 0.033 \ \rm ps^{-1} = (2.87 \pm 0.22)\ 10^{-4}\ eV/c^2\ .$$

This is consistent with the current world average $0.474 \pm 0.031\,\rm ps^{-1}$ [21], and supersedes previous ALEPH results on Δm_d.

Acknowledgements

We would like to thank our colleagues in the accelerator divisions of CERN for the excellent performance of the LEP accelerator. Furthermore we would like to thank the technical personnel of CERN and the collaborating institutions for their support in constructing and maintaining the experiment. Those of us from non-member states thank CERN for its hospitality.

References

[1] D. Buskulic *et al.* (ALEPH Collaboration), Phys. Lett. **B 313** (1993) 498.

[2] D. Buskulic *et al.* (ALEPH Collaboration), Phys. Lett. **B 322** (1994) 441.

[3] P. D. Acton *et al.* (OPAL Collaboration), Phys. Lett. **B 327** (1994) 411.

[4] R. Akers *et al.* (OPAL Collaboration), Phys. Lett. **B 336** (1994) 585;
P. Abreu *et al.* (DELPHI Collaboration), Phys. Lett. **B 338** (1994) 409.

[5] D. Buskulic *et al.* (ALEPH Collaboration), Nucl. Instr. Meth. **A 294** (1990) 121.

[6] D. Buskulic *et al.* (ALEPH Collaboration), Nucl. Instr. Meth. **A 360** (1995) 481.

[7] D. Buskulic *et al.* (ALEPH Collaboration), Nucl. Instr. Meth. **A 346** (1994) 461.

[8] D. Buskulic *et al.* (ALEPH Collaboration), Z. Phys. **C 62** (1994) 179.

[9] T. Sjöstrand and M. Bengtsson, Comput. Phys. Commun. **43** (1987) 367.

[10] D. Buskulic *et al.* (ALEPH Collaboration), Phys. Lett. **B 284** (1992) 177.

[11] D. Buskulic *et al.* (ALEPH Collaboration), Phys. Lett. **B 313** (1993) 535.

[12] D. Buskulic *et al.* (ALEPH Collaboration), CERN PPE/96-014 "Improved Measurement of the $\overline{B}^0$ and B^- Meson Lifetimes", submitted to Z. Phys. C.

[13] H.-G. Moser, "B lifetimes at LEP", to appear in Proc. of the EPS Conf. on HEP, Brussels, Belgium (July 1995).

[14] L. Montanet *et al.* (Particle Data Group), Phys. Rev. D **50** (1994) 1173.

[15] S. Bethke *et al.* (JADE Collaboration), Phys. Lett. **B 213** (1988) 235.

[16] D. Buskulic *et al.* (ALEPH Collaboration), CERN PPE/96-072, "Measurement of the b Forward-Backward Asymmetry and Mixing Using High-$p_{\rm T}$ Leptons", to appear in Phys. Lett. B.

[17] D. Buskulic *et al.* (ALEPH Collaboration), Phys. Lett. **B 356** (1995) 409.

[18] S. L. Wu, "Recent Results on B Meson Oscillations", to appear in Proc. of Int. Symp. on Lepton-Photon Interactions, Beijing, China (August 1995).

[19] D. Buskulic *et al.* (ALEPH Collaboration), CERN PPE/96–09, "Determination of $\sin^2\theta^{\rm eff}_{\rm W}$ Using Jet Charge Measurements in Hadronic Z Decays", to appear in Z. Phys. C.

[20] S. Emery, "Etude de la dépendance temporelle des oscillations $B^0 - \overline{B}^0$ par la méthode de la charge du jet sur l'expérience ALEPH", PhD thesis, CE-Saclay (1995).

[21] R.M. Barnett *et al.* (Particle Data Group), Phys. Rev. D **54** (1996) 1, preview available on WWW (http://pdg.lbl.gov).